JOURNAL OF CATALYSIS 145, 65–72 (1994)

Coupling of Oxidative Dehydrogenation and Aromatization Reactions of Butane

Wen-Qing Xu* and Steven L. Suib*,†,‡,[1]

*Department of Chemistry, †Department of Chemical Engineering, and ‡Institute of Materials Science, University of Connecticut, Storrs, Connecticut 06269-3060

Received March 19, 1993; revised August 4, 1993

Coupling of oxidative dehydrogenation and aromatization of butane by using a dual function catalyst has led to a significant enhancement of the yields (from 25 to 40%) and selectivities to aromatics (from 39 to 64%). Butane is converted to aromatics by using either zinc-promoted [Ga]–ZSM-5 or zinc and gallium copromoted [Fe]–ZSM-5 zeolite as a catalyst. However, the formation of aromatics is severely limited by hydrocracking of butane to methane, ethane, and propane due to the hydrogen formed during aromatization reactions. On the other hand, the oxidative dehydrogenation of butane to butene over molybdate catalysts is found to be accompanied by a concurrent undesirable reaction, i.e., total oxidation. When two of these reactions (oxidative dehydrogenation and aromatization of butane) are coupled by using a dual function catalyst they have shown to complement each other. It is believed that the rate-limiting step for aromatization (butane to butene) is increased by adding an oxidative dehydrogenation catalyst (Ga–Zn–Mg–Mo–O). The formation of methane, ethane, and propane was suppressed due to the removal of hydrogen initially formed as water. Studies of ammonia TPD show that the acidities of [Fe]–ZSM-5 are greatly affected by the existence of metal oxides such as Ga_2O_3, MgO, ZnO, and MoO_3.

I. INTRODUCTION

Zinc- or gallium-promoted ZSM-5 zeolite catalysts can selectively transform light hydrocarbons to aromatics (1–9). Metal cations are efficient catalytic species for dehydrogenation of intermediate alkenes into aromatics (2, 3, 5, 10, 11). Ga_2O_3 is active for the dehydrogenation of propane at low conversions (12). A dual-site (metal cation, acid) mechanism for the activation of alkanes was proposed by Meriaudeau and Naccaache (13). Ono and his co-workers concluded that metal cations and acidic sites are exclusively responsible for the activation of ethane and the activation of pentane or hexane, respectively (4). Activation of butane and propane are enhanced by both types of sites (14–16). Hydrogen back-spillover was proposed so that hydrogen is transferred from zeolitic acid sites to the metal oxide surface which is located on the outside of the zeolite particles. These acidic and metal oxide sites do not have to be adjacent to each other for promoting the formation of aromatics (12, 17–22).

In the conversion of propane and butane to aromatics, activation of these alkanes by dehydrogenation to alkene intermediates is a limiting step since alkene feeds show high activity and selectivity to aromatics (10, 11). Reactant feeds containing 5% oxygen increase the conversion and enhance the selectivity to aromatics (23). However, feeds containing hydrogen increase the formation of methane and ethane and cause the selectivity to aromatics to drop (24). Palladium membranes have been used in an aromatization reactor to remove the hydrogen that is produced from dehydroaromatization of butane (25). The conversion and selectivity to aromatics were improved greatly with these membranes. However, one disadvantage of this technique is that the palladium membranes need to be regenerated after they lose their ability to sorb hydrogen.

Dehydrogenation reactions of *n*-butane are equilibrium limited (26) and catalysts tend to rapidly lose their activity due to severe coking. Oxidative dehydrogenation of butane is thermodynamically favored over dehydrogenation reactions. Coking becomes less severe in the presence of oxygen. The feasibility of oxidative dehydrogenation of *n*-butane was established by McDonald and McIntyre (27) over a molybdic oxide–aluminum phosphate catalyst. Stepanov *et al.* (28) extensively studied this reaction for binary oxide systems of molybdenum oxide. Mg–Mo, Ni–Mo, and Co–Mo were considered to be selective oxide catalysts (28, 29). V–Mg–O and orthovanadates were reported to be comparable with molybdenum containing catalysts with respect to activity and selectivity (30, 31). Iron-doped (32) and phosphinated (33, 34) Bi–Mo–Al catalysts were also studied and no improvement in selectivity was observed as compared to Mg–Mo systems. In molyb-

[1] To whom correspondence should be addressed.

0021-9517/94 $5.00

denum-containing systems, Mg–Mo complex oxides are very active and the most selective for formation of butene and butadiene (28, 35, 36). When the ratio of oxygen to *n*-butane decreases, the conversion of *n*-butane drops; however, the selectivities to butenes and butadiene are improved (30). From the literature (28, 35, 36), it seems that it is difficult to obtain selectivities to butenes and butadiene greater than 60% due to the concurrent total oxidation reaction.

The general idea of this study is to use a dual function catalyst in order to couple aromatization and oxidative dehydrogenation reactions of butane. [Ga]–ZSM-5 and [Fe]–ZSM-5 were used as zeolite components for the aromatization catalysts. Mg–Mo–O was chosen as an oxidative dehydrogenation catalyst. The interactions of these two types of catalysts were studied. Complementary effects were observed for these coupled systems by mixing GaZn[Fe]–ZSM-5 aromatization catalysts with Ga–Zn–Mg–Mo–O oxidative dehydrogenation catalysts.

II. EXPERIMENTAL

[Fe]–ZSM-5 zeolites were synthesized and characterized according to literature procedures (37, 38). An aqueous solution of sodium silicate was slowly added to an acidic solution of ferric chloride followed by addition of tetrapropylammonium bromide. The mixture was then autoclaved for 5 days at 170°C. The recovered product was calcined at 500°C for 4 h in nitrogen and for 4 more hours in air and ion-exchanged with an aqueous solution of 1 *M* ammonium nitrate followed by 4 h calcination in air. Two [Fe]–ZSM-5 zeolites with Si/Fe equal to 40 and 76 were obtained. These two samples were ion-exchanged with 1 *M* ammonium nitrate solution, filtered and dried at 110°C overnight to obtain NH_4[Fe]–ZSM-5. [Ga]–ZSM-5 was prepared with gallium nitrate, tetraethoxysilane, and tetrapropylammonium bromide by adjusting the initial pH to 10.0. This mixture was autoclaved at 170°C for 5 days. The white product was calcined at 550°C for 4 h under nitrogen and 2 h under air to generate the H form of [Ga]–ZSM-5. The ratio of silicon to gallium for [Ga]–ZSM-5 is 37 as determined by atomic absorption (AA) methods. All of these zeolite materials have been characterized by XRD, FTIR, Mössbauer, EPR, TGA, DSC, and AA analyses (39).

Only [Fe]–ZSM-5 (Si/Fe = 76) was used for doping with gallium and zinc promoters. Ga[Fe]–ZSM-5 (Fe/Ga = 1.2) was prepared by ion-exchanging NH_4[Fe]–ZSM-5 with 1 *N* gallium nitrate solution for 4 h. NH_4[Fe]–ZSM-5 was co-ion-exchanged with an aqueous solution of 0.5 *N* gallium nitrate and 0.5 *N* zinc nitrate for 4 h to produce GaZn[Fe]–ZSM-5 (Fe/Ga/Zn = 9.8 : 5.0 : 1). Zn[Ga]–ZSM-5 (Ga/Zn = 2.3) was obtained by ion-exchange of [Ga]–ZSM-5 with a 1 *N* zinc nitrate solution. These samples were then dried at 110°C overnight and calcined at 550°C for 4 h.

The Mg–Mo–O sample was prepared by evaporating a mixture of ammonium paramolybdate solution with magnesium oxide which was prepared by calcining magnesium carbonate at 700°C for 4 h. The resultant white product (MgO) was mixed with water and stirred for 14 h, followed by addition of ammonium paramolybdate solution. This mixture was evaporated at 80°C until a thick slurry is formed, dried at 110°C overnight, and transferred to a furnace for 2 h calcination at 580°C. The resultant sample is labelled Mg–Mo–O and has a Mg/Mo ratio of 9.18. Some of this sample (Mg–Mo–O) was further stirred with a nitrate solution containing 5 wt% ZnO and 5 wt% Ga_2O_3, evaporated, dried, and calcined at 580°C for 2 h. The resultant sample is labelled Ga–Zn–Mg–Mo–O which has a Ga/Zn/Mg/Mo ratio of 1.00 : 1.14 : 33.4 : 3.64.

X-ray diffraction experiments were done on a Scintag Model PDS 2000 diffractometer with a monochromatic X-ray beam and scintillator. Samples were mounted on an aluminum plate that remained horizontal during all experiments. A beam voltage of 45 kV and a current of 40 mA were used with Cu $K\alpha$ radiation.

Scanning electron microscopy (SEM) and energy dispersive X-ray (EDX) analyses were done on an Amray Model 1810 D microscope with an Amray PV 9800 energy dispersive X-ray analyzer, which is equipped with a windowless detector for observation of elements with atomic numbers below Na and greater than Be.

Temperature-programmed desorption (TPD) of ammonia experiments were done on a home-made TPD apparatus (40). The samples were heated from room temperature to 550°C at a ramping rate of 15°C/min and this temperature was kept for 1 h under 30 ml/min of ultrapure helium gas, followed by cooling to 100°C. Ammonia was introduced into the sample and kept flowing for 30 min. The samples were purged with helium for 40 min in order to eliminate physisorbed species. The temperature was ramped at 15°C/min from 100 to 610°C and TPD spectra of ammonia were acquired. The amount of desorbed ammonia is deduced by calibration of desorption peaks with a sampling loop having a volume of 34.4 μmol.

Pulse reaction techniques were used to evaluate the catalytic properties of the above-mentioned catalysts. The ultrapure helium was fed through a pulse reactor at a flow rate of 15 ml(STP)/min. Each catalyst (200 mg) was treated with oxygen at 550°C for 30 min followed by helium purging for 1 h. Each injected pulse contained 39.8 μl of *n*-butane. Liquid-nitrogen traps were used to trap all effluents except methane. After removing the cold trap, the condensates were evaporated and carried into a Varian Aerograph Series 1400 GC for separation.

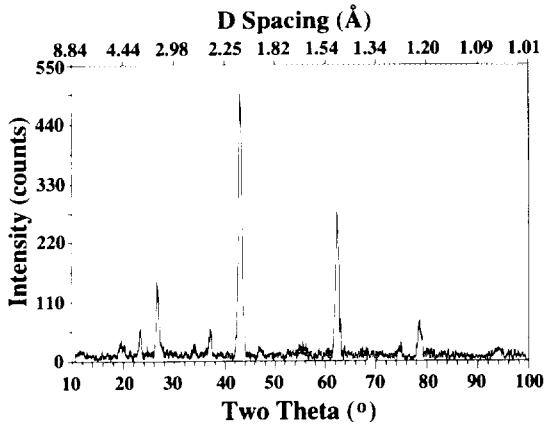

FIG. 1. X-ray diffraction pattern of sample Mg–Mo–O.

III. RESULTS

X-Ray Diffraction Analyses

The XRD pattern of sample Mg–Mo–O is shown in Fig. 1. Lines at *d* spacings of 2.42, 2.10, 1.49, 1.26, 1.21, and 1.05 Å are due to diffraction peaks of cubic magnesium oxide (ASTM card 4-829). Lines at *d* spacings of 4.52, 4.17, 3.81, 3.32, and 2.63 Å are due to monoclinic magnesium molybdate (ASTM card 21-961). No diffraction line is observed which is due to molybdenum oxide in this XRD pattern. Sample Ga–Zn–Mg–Mo–O has an XRD pattern similar to sample Mg–Mo–O. No line characteristic of zinc oxide and gallium oxide is observed since the content of zinc or gallium oxide is too small.

The Interactions of [Fe]–ZSM-5 with Various Oxides

A. Acidity. [Fe]–ZSM-5 catalyst (10 mg) with a Si/Fe equal to 40 was mixed with 10 mg of several oxides such as Ga_2O_3, MgO, ZnO, and MoO_3, respectively, and this mixture was then calcined in helium at 550°C for 8 h. Ammonia TPD spectra were obtained for these mixtures, as shown in Fig. 2. [Fe]–ZSM-5 itself (Fig. 2b) has two

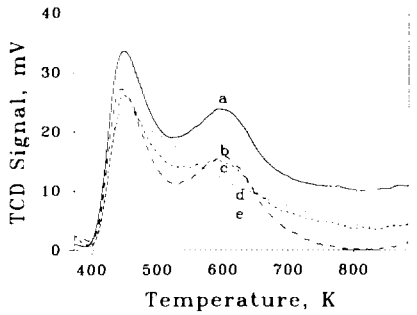

FIG. 2. Ammonia TPD of [Fe]–ZSM-5 (Si/Fe = 40): (a) + Ga_2O_3, (b) precursor, (c) + MgO, (d) + ZnO, and (e) + MoO_3.

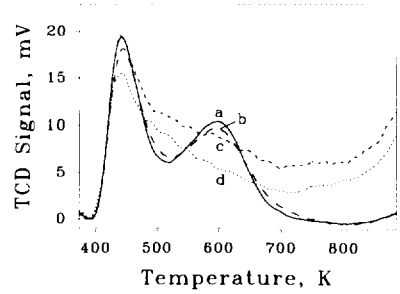

FIG. 3. Ammonia TPD of [Fe]–ZSM-5 (Si/Fe = 76): (a) precursor, (b) GaZn-doped, (c) GaZn-doped + Mg–Mo–O, and (d) GaZn-doped + Ga–Zn–Mg–Mo–O.

TPD peaks at 444 K and 598 K. Ga_2O_3 does not seem to change acidic strength with respect to peak positions, but there is a baseline shift (Fig. 2a). The [Fe]–ZSM-5 catalyst mixed with MgO shows two TPD peaks that are broadened (Fig. 2c). The interaction of [Fe]–ZSM-5 and ZnO (Fig. 2d) results in coalescence of two peaks. The overall number of acid sites is not obviously reduced by adding either MgO or ZnO. However, addition of MoO_3 destroys some of the high-temperature acid sites of [Fe]–ZSM-5 (Fig. 2e).

Figure 3 shows ammonia TPD data for [Fe]–ZSM-5 with Si/Fe equal to 76 after exchange of Zn^{2+} and Ga^{3+} ions and after mixing with Mg–Mo–O and Ga–Zn–Mg–Mo–O oxidative dehydrogenation catalysts. Low iron content [Fe]–ZSM-5 has two ammonia TPD peaks (Fig. 3a) as the high iron content catalyst (Fig. 2b). After co-exchange of the [Fe]–ZSM-5 (Si/Fe = 76) with 0.5 N Zn^{2+} and 0.5 *N* Ga^{3+} solutions, the TPD peak shows some broadening (Fig. 3b), but the number of acidic sites seems to remain the same as that for [Fe]–ZSM-5. When GaZn[Fe]–ZSM-5 (Si/Fe = 76) zeolite was mixed with an oxidative dehydrogenation catalyst (Mg–Mo–O) the high temperature peak disappears and a broad distribution of acid sites is observed (Fig. 3c). Integration of the desorption curve up to the temperature of 800 K leads to a result that the number of acidic sites for such mixture is about 29% more than that for GaZn[Fe]–ZSM-5. The same thing happened for a mixture of GaZn[Fe]–ZSM-5 (Si/Fe = 76) zeolite and Ga–Zn–Mg–Mo–O (Fig. 3d). However, the total number of acid sites in this material (Fig. 3d) is markedly (about 27%) reduced as compared to the mixture of Mg–Mo–O and GaZn[Fe]–ZSM-5 (Si/Fe = 76) (Fig. 3c).

B. SEM–EDX Analyses. GaZn[Fe]–ZSM-5 has an EDX spectrum shown in Fig. 4a. This sample contains oxygen, silicon, iron, zinc, and gallium. The mixture of this sample with an oxidative dehydrogenation catalyst (Mg–Mo–O) has been studied by butane pulse reactions (see below). SEM spot analysis of a zeolite particle results

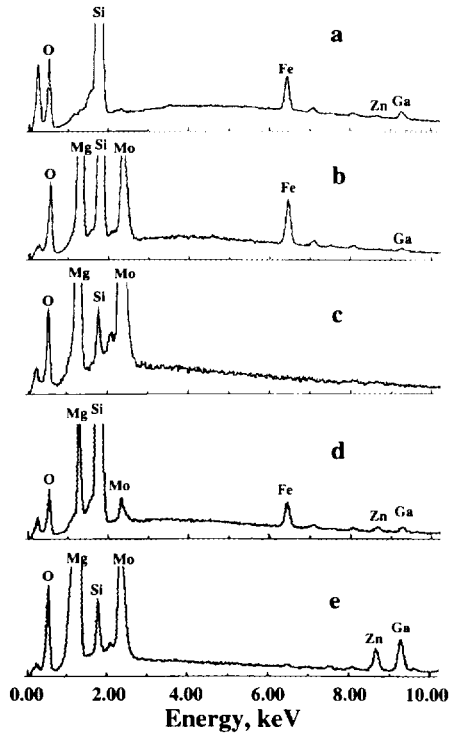

FIG. 4. SEM–EDX Analysis of [Fe]–ZSM-5 (Si/Fe = 76): (a) GaZn-doped; (b) zeolite particle, GaZn-doped + Mg–Mo–O; (c) oxide particle, GaZn-doped + Mg–Mo–O; (d) zeolite particle, GaZn-doped + Ga–Zn–Mg–Mo–O; and (e) oxide particle, GaZn-doped + Ga–Zn–Mg–Mo–O.

in an EDX pattern (Fig. 4b) that shows the disappearance of zinc but the presence of gallium. Spot analysis of an Mg–Mo–O particle of the same sample as Fig. 4b shows that there is no observation of zinc or gallium (Fig. 4c). Furthermore, EDX data on a zeolite particle for the mixture of GaZn[Fe]–ZSM-5 and Ga–Zn–Mg–Mo–O show the presence of zinc and gallium (Fig. 4d). These data suggest that zinc and gallium are associated with zeolite particles. The oxide particles contain Mg, Mo, Zn, and Ga (Fig. 4e).

Pulse Reaction Experiments

A. Zinc and gallium copromotion and hydrogen and oxygen effects. The [Ga]–ZSM-5 sample with Si/Ga equal to 37 was used for butane pulse reaction studies. Zn^{2+} ion-exchanged [Ga]–ZSM-5 samples were activated with two different gases, hydrogen and oxygen. For these samples, results of five pulses of butane showed that the catalysts are quite stable based on conversion and selectivity. The results of Fig. 5 are from the third butane pulse. The products formed in these aromatization reactions are methane, ethane, ethylene, propane, propylene, and butenes in addition to aromatics such as benzene, toluene, xylenes, and ethylbenzene. Fresh catalysts, initially colored white, become gray after pulse reaction experiments. These data indicate that coke formation and cracking of butane to light hydrocarbons are main side reactions for butane aromatization.

For cracking of butane to C1 to C3 products (Fig. 5a), [Ga]–ZSM-5 is the most active among three samples, i.e., [Ga]–ZSM-5, hydrogen activated Zn[Ga]–ZSM-5, and oxygen activated Zn[Ga]–ZSM-5. Hydrogen-activated Zn[Ga]–ZSM-5 is less active for cracking of butane. Oxygen-activated Zn[Ga]–ZSM-5 is the least active for cracking of butane among these three samples. The cracking of butane to lower hydrocarbons is increased by increasing the reaction temperature for zinc-promoted [Ga]–ZSM-5 materials activated either by hydrogen or by oxygen. But for [Ga]–ZSM-5 itself, cracking of butane is decreased with increasing the reaction temperature. The reason for this may be due to high conversions of butane (over 90%, see below) for [Ga]–ZSM-5 at temperatures of 550 to 650°C. The production of *n*-butenes decreases with an increase of reaction temperature (Fig. 5b). Moreover, differences among these three [Ga]–ZSM-5 samples have obviously been observed. For example, [Ga]–ZSM-5 has the lowest ability of three to produce *n*-butenes. Oxygen-activated Zn[Ga]–ZSM-5 is more active, whereas the hydrogen-activated Zn[Ga]–ZSM-5 produces the most *n*-butenes. For formation of aromatics (Fig. 5c), yield is increased as reaction temperature increases. The oxygen-activated Zn[Ga]–ZSM-5 catalyst produces the most aromatics of the three [Ga]–ZSM-5 materials. The hydrogen-activated Zn[Ga]–ZSM-5 catalyst shows intermediate yields of aromatics. [Ga]–ZSM-5 itself shows the lowest activity for the formation of aromatics. Conse-

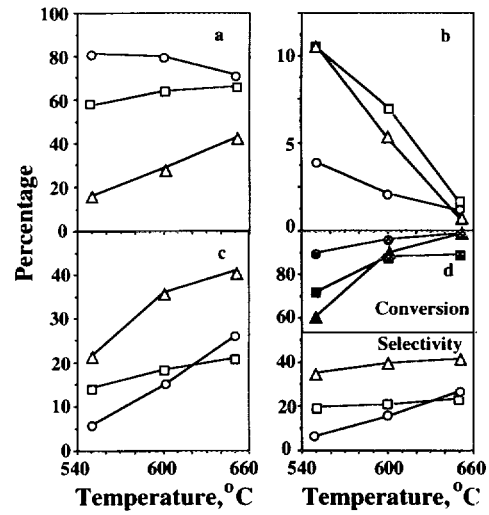

FIG. 5. Butane pulse reactions of ○, [Ga]–ZSM-5; □, hydrogen-activated Zn[Ga]–ZSM-5; and Δ, oxygen-activated Zn[Ga]–ZSM-5; (a) C1 to C3, (b) *n*-butenes, (c) aromatics, and (d) conversion of butane (top) and selectivity to aromatics (bottom).

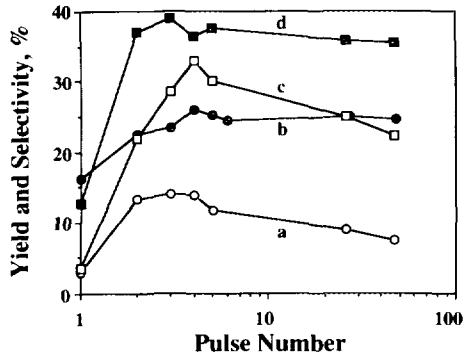

FIG. 6. Butane Pulse Reactions of [Fe]–ZSM-5 (Si/Fe = 76) at 550°C: (a) aromatic yield for Ga-doped, (b) aromatic yield for GaZn-doped, (c) selectivity to aromatics for Ga-doped, and (d) selectivity to aromatics for GaZn-doped.

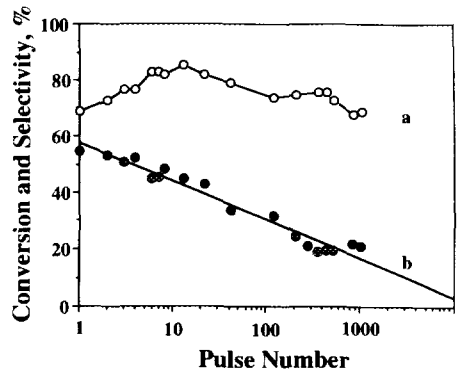

FIG. 7. Butane pulse reactions of Mg–Mo–O at 550°C: (a) selectivity to butenes and (b) conversion of butane.

quently, among these three samples, [Ga]–ZSM-5 is the most active for butane conversion, but least selective to aromatics (Fig. 5d). Oxygen-activated Zn[Ga]–ZSM-5 is the most selective for aromatics. With an increase of reaction temperature, the activity for oxygen-activated Zn[Ga]–ZSM-5 increases more rapidly than the hydrogen-activated Zn[Ga]–ZSM-5. The conversions for oxygen and hydrogen-activated Zn–[Ga]–ZSM-5 are reversed (i.e., oxygen activated > hydrogen activated) around 600°C.

One of our hypotheses was that if [Fe]–ZSM-5 zeolite was used and the ferric valence could change between 3+ to 2+, more oxygen might be available than for [Ga]–ZSM-5. Results of butane pulse reactions at 550°C for various [Fe]–ZSM-5 samples are shown in Fig. 6. The yield and selectivity for aromatics change with pulse number. Initially, it seems that extraframework Fe^{3+} is reduced and some butane is converted to carbon dioxide. Yield and selectivity to aromatics increase with pulse number and then slowly decrease. For the Ga^{3+} and Zn^{2+} coexchanged [Fe]–ZSM-5 catalyst (Fig. 6b), better activity for aromatics is observed than for Ga^{3+} ion-exchanged [Fe]–ZSM-5 (Fig. 6a). GaZn[Fe]–ZSM-5 has higher selectivity (Fig. 6d) than Ga[Fe]–ZSM-5 (Fig. 6c). The above results (Fig. 5 and Fig. 6) clearly indicate that Ga^{3+} and Zn^{2+} show a copromotion effect for butane conversion to aromatics.

B. Butane pulse reactions for Mg–Mo–O samples. Figure 7 shows results of butane pulse reactions at 550°C for the Mg–Mo–O sample. In addition to butene formation, side reactions occurred, such as total oxidation and cracking of butane to C1, C2, and C3. The selectivity to butene ranges from 70 to 85% (Fig. 7a). The selectivity to butene is initially increased as the pulse number increases due to a decrease of total oxidation with increasing pulse number. Further injection of butane consumes more oxygen of the Mg–Mo–O catalyst, therefore, the activity decreases (Fig. 7b). On the other hand, the partially reduced Mg–Mo–O causes the selectivity to butenes to drop with increasing pulse number due to cracking. Sample Ga–Zn–Mg–Mo–O showed similar results for butane pulse reactions.

C. Coupling of aromatization and oxidative dehydrogenation. The aromatization catalyst (GaZn[Fe]–ZSM-5) and the oxidative dehydrogenation catalyst sample (Mg–Mo–O) were mixed. Results of butane pulse reactions at 550°C are shown in Fig. 8. The yield of aromatics for coupled catalysts (Fig. 8d) drops more than 50% as compared to the aromatization catalyst by itself (Fig. 8c) from the first pulse to the 50th pulse. The decrease in the aromatic yield results in a similar decrease in the selectivity to aromatics, as shown in Figs. 8a and 8b.

The oxidative dehydrogenation catalyst (Mg–Mo–O) was also impregnated with 5 wt% ZnO and 5 wt% Ga_2O_3 with nitrate precursors. After calcination at 580°C for 2 h, this oxidative dehydrogenation catalyst was mixed with the aromatization catalyst (GaZn[Fe]–ZSM-5). The bu-

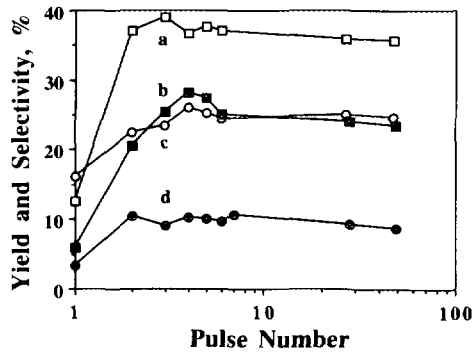

FIG. 8. Butane pulse reactions of GaZn[Fe]–ZSM-5 (Si/Fe = 76) at 550°C: (a) selectivity to aromatics for the precursor, (b) selectivity to aromatics for the precursor + Mg–Mo–O, (c) aromatic yield for the precursor, and (d) aromatic yield for the precursor + Mg–Mo–O.

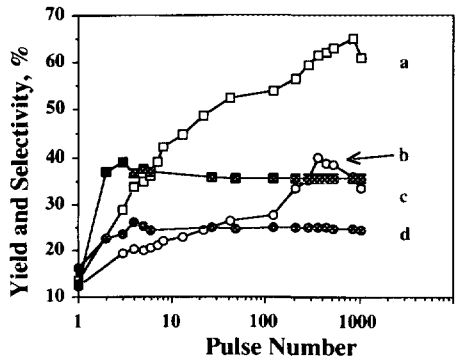

FIG. 9. Butane pulse reactions at 550°C: (a) selectivity to aromatics for GaZn[Fe]–ZSM-5 (Si/Fe = 76) + Ga–Zn–Mg–Mo–O, (b) total yield of aromatics for GaZn[Fe]–ZSM-5 (Si/Fe = 76) + Ga–Zn–Mg–Mo–O, (c) selectivity to aromatics for GaZn[Fe]–ZSM-5 (Si/Fe = 76), and (d) yield of aromatics for GaZn[Fe]–ZSM-5 (Si/Fe = 76).

tane pulse reactions at 550°C show quite different results (Fig. 9) from the previously-mentioned results (Fig. 8d, mixing GaZn[Fe]–ZSM-5 and Mg–Mo–O). With pulse number increasing, the yield (Fig. 9b) and selectivity (Fig. 9a) of aromatics both increase, reach a maximum, and then drop. The formation of benzene almost stays at the same level. The formation of toluene increases as the pulse number increases. When C8 aromatics start to form, the total yield of aromatics (Fig. 9b) and the selectivity to aromatics (Fig. 9a) reach a maximum (40.0 and 64%, respectively). The composition of aromatics for such maximum is 20.5% benzene, 15.3% toluene, and 4.2% xylenes. The yields of aromatics (Fig. 9d) and the selectivities to aromatics (Fig. 9c) for GaZn[Fe]–ZSM-5 were also plotted out for the sake of easy comparison.

IV. DISCUSSION

In butane pulse reactions (Fig. 5d), [Ga]–ZSM-5 shows high activity for butane conversion, however, low selectivity to aromatics. After introduction of zinc cations into [Ga]–ZSM-5 by ion-exchange, the conversion for butane drops and selectivities to aromatics are improved to different extents depending on activation conditions. Activation with oxygen leads to more production of aromatics than with hydrogen (Fig. 5c). This implies that gallium and zinc are copromoters for butane aromatization leading to enhanced yields and selectivities to aromatics. Even though the effects of oxygen interactions are not clear at this stage, these results suggest that the oxygen-activated sample may help speed up the limiting step (dehydrogenation) for aromatization and suppresses hydrocracking processes due to hydrogen formed in the aromatization process. For example, data of Fig. 5 show that the oxygen-activated sample has less formation of C1, C2, and C3 (Fig. 5a). Oxygen-activated samples also lead to a little less butene formation (Fig. 5b), which may suggest that oxygen-activated samples are more capable of transforming butene intermediates into aromatics. These results are consistent with literature reports (23) that reactant feeds containing 5% oxygen increase butane conversion and enhance selectivity to aromatics.

From the above results, it seems reasonable that use of an [Fe]–ZSM-5 catalyst may offer more capability to store oxygen. The oxidative ability of Ga[Fe]–ZSM-5 at 550°C is strong enough to have some butane totally oxidized for the first pulse as shown in Fig. 6. A low yield and selectivity to aromatics are observed. After oxygen is consumed in the first pulse via total oxidation, the yield of aromatics and selectivity to aromatics are improved in continuing pulses. Ga[Fe]–ZSM-5 also has a better yield of aromatics (Fig. 6a) and better selectivity to aromatics (Fig. 6c) at reaction temperature of 550°C as compared to [Ga]–ZSM-5 (Figs. 5e and 5f, respectively). Gallium and zinc copromotion for aromatization is also observed in the [Fe]–ZSM-5 system which leads to enhanced yields (Figs. 6a and 6b) and selectivities to aromatics (Figs. 6c and 6d).

Our major focus was to introduce an oxidative dehydrogenation catalyst into the aromatization system. In the molybdenum-containing system, Mg–Mo–O has been suggested to be a very active and selective catalyst for the oxidative dehydrogenation of butane to butene and butadiene (28, 35, 36). The best composition (36) (MgO/MoO_3 = 9.18) was chosen as regards conversion and selectivity and was prepared by an evaporation method. The XRD pattern of Mg–Mo–O (Fig. 1) showed that it contains magnesium oxide and magnesium molybdate. High selectivity for oxidative dehydrogenation instead of oxygenate formation is partially attributed to the basic surface of magnesium oxide which facilitates desorption of basic butenes and butadiene (30). For Mg–V–O catalysts, Kung and co-workers (30) have reported that the absence of V=O lowers the oxidation activity of the surface, which is another factor for improving oxidative dehydrogenation of butane. Thus the presence of magnesium molybdate instead of molybdenum oxide in the catalyst Mg–Mo–O may be responsible for the oxidative dehydrogenation of butane. Consequently, our butane pulse reaction results (Fig. 7) also show that Mg–Mo–O is able to oxidatively dehydrogenate butane. The selectivity to *n*-butenes ranges from 70 to 85% (Fig. 7a). The activity drops as pulse number increases since lattice oxygen in Mg–Mo–O is consumed during every pulse (Fig. 7b). The reduction of Mg–Mo–O is therefore a first order process with a time unit equal to the period of each butane pulse.

Oxidative dehydrogenation (Mg–Mo–O) and aromatization (GaZn[Fe]–ZSM-5) catalysts when coupled together show a significant loss of zinc evidenced by

SEM–EDX analyses (Fig. 4). Zinc ions may either migrate out of the zeolite or be reduced by hydrocarbon and sublimed out of the system at reaction temperature. Another possibility is that zinc ions may be buried deeper than the depth of analysis of EDX. The loss of gallium ions occurs but is not significant. In any event, losing zinc and gallium ions results in dramatic decrease in the yield of aromatics (Fig. 8d) by a factor of 2 as compared to GaZn[Fe]–ZSM-5 (Fig. 8c), instead of enhancing aromatization as expected.

In order to retain zinc and gallium ions in the system, 5 wt% ZnO and 5 wt% Ga_2O_3 are further added to the Mg–Mo–O system. EDX analyses (Fig. 4d) provide evidence that zinc and gallium are associated with zeolite [Fe]–ZSM-5 when GaZn[Fe]–ZSM-5 is mixed with Ga–Zn–Mg–Mo–O. Coupling of oxidative dehydrogenation and aromatization reactions is then successful (Fig. 9). The yield (Fig. 9b) and selectivity (Fig. 9a) to aromatics increase with increasing pulse number. The highest yield is as high as 40% and the selectivity to aromatics is as high as 64%. Thus the limiting step for aromatization (dehydrogenation of butane) is enhanced by addition of an oxidative dehydrogenation component containing ZnO and Ga_2O_3. This lead to greater formation of aromatics. On the other hand, the oxidative dehydrogenation component abstracts hydrogen to form water, which results in less hydrocracking and concomitant higher selectivity to aromatics. For oxidative dehydrogenation, butene or butadiene products that are formed are consumed immediately in the aromatization process so that total oxidation can be suppressed to a certain degree. As a reviewer has pointed out, a continuous increase in selectivity to aromatics with an increase of pulse number should have some relationship to changes in catalyst properties. Coke deposition was one of the changes for the used catalyst. The acidity of the zeolite and the chemical states for zinc, gallium, and molybdenum might be influenced after successive pulses of butane and finally can be optimized for this coupled system.

In the conversion of butane to aromatics, activation of butane to butene intermediates is a limiting step (10, 11). Both metal cations and acidic sites are necessary for activation of butane (14–16). Reactions of aromatization for three types of catalysts such as Ga^{3+} promoted, Ga^{3+} and Zn^{2+} copromoted, and the coupled system are shown in Scheme I. For gallium-promoted aromatization catalysts (Route A), Ga^{3+} initially abstracts a hydride ion from butane to form a carbocation. The carbocation interacts with Brønsted acidic sites so that acidic protons combine with hydride ion to form hydrogen which causes butane to crack to lower alkanes. The carbocation adsorbs on Brønsted acidic sites. This adsorbed carbocation leads to formation of butene intermediates. Moreover, the presence of Ga^{3+} and Zn^{2+} (Route B), instead of Ga^{3+} itself, speeds up the abstraction of hydride ion from butane so

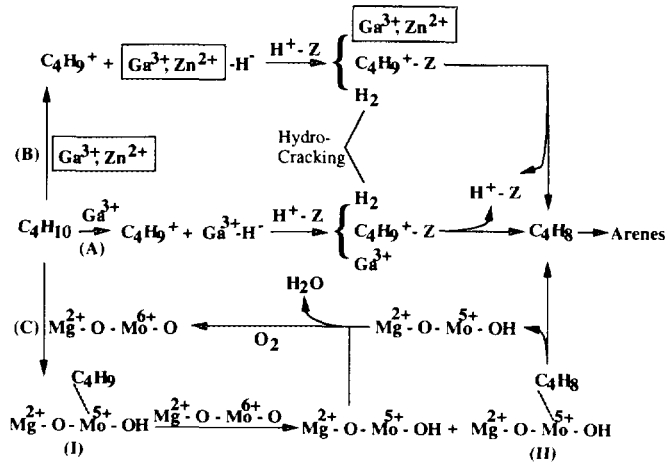

Scheme I. Reaction pathways for butane aromatization on ZSM-5 zeolites (A) Ga^{3+}-promoted, (B) Ga^{3+} and Zn^{2+} copromoted, and (C) coupling of oxidative dehydrogenation catalysts.

that the yields and selectivities to aromatics are enhanced significantly. For example, Zn[Ga]–ZSM-5 has a 21% yield and 37% selectivity to aromatics at 550°C, while [Ga]–ZSM-5 only has a 6% yield and 7% selectivity to aromatics at 550°C (Figs. 5c and 5d). Furthermore, activation of butane to butene intermediates (limiting step for aromatization) is accelerated by coupling of oxidative dehydrogenation and aromatization (Route C). A mechanism similar to the Mars–van Krevelen mechanism is proposed to explain the oxidation of butane to butene intermediates for aromatization. Mg^{2+}–O–Mo^{6+}–O abstracts a hydrogen atom from butane to form I (see Scheme I). Another Mg^{2+}–O–Mo^{6+}–O further abstracts the second hydrogen from adsorbed C_4H_9 to form II (see Scheme I) which then desorbs butenes as intermediates for aromatization and Mg^{2+}–O–Mo^{5+}–OH. Two Mg^{2+}–O–Mo^{5+}–OH species can then interact with each other to form water and are reoxidized by gaseous oxygen back to Mg^{2+}–O–Mo^{6+}–O. Through this reaction route, the yields and selectivities to aromatics can reach 40 and 64%, respectively, for the coupled system (GaZn [Fe]–ZSM-5 + Ga-Zn–Mg–Mo–O, Figs. 9c and 9b). Note that GaZn–[Fe]–ZSM-5 for comparison only has a 25% yield and 39% selectivity to aromatics (Figs. 9d and 9c, respectively). Metal cations such as Ga^{3+} and Zn^{2+} are efficient catalytic species for dehydrogenation of butene intermediates to aromatics (2, 3, 5, 10, 11). The formation of hydrogen in transforming butene intermediates to aromatics may also be removed by the presence of oxidative dehydrogenation catalysts.

The interactions of [Fe]–ZSM-5 and various oxides have been studied by ammonia TPD (Figs. 2 and 3). These data suggest that the acidity of such zeolites can be modified by different oxides. In particular, the populations of

high-temperature acid sites can be redistributed to lower temperature acid sites. The cause of the change in ammonia TPD data shown in Fig. 2 is not well understood at this stage. However, it is believed that the catalyst would lose its activity for aromatization if the acidity of the zeolite is completely eliminated by mixing with metal oxide (Ga–Zn–Mg–Mo–O).

V. CONCLUSION

Zinc and gallium ions can copromote butane aromatization reactions. Oxygen activation of Zn[Ga]–ZSM-5 can improve the yield and selectivity to aromatics. After mixing an oxidative dehydrogenation component containing ZnO and Ga_2O_3 with an aromatization catalyst, the yield and selectivity to aromatics are enhanced significantly. It is believed that the rate of the limiting step for aromatization is sped up by this coupled system with a corresponding suppression of hydrocracking by removing hydrogen that is formed. Kinetic studies of continuous flowing coupled reactions of oxidative dehydrogenation and aromatization of butane will be the subject of further investigations. These studies suggest that interactions between [Fe]–ZSM-5 and different oxides occur and zeolite acidity can be modified by different oxides.

ACKNOWLEDGMENTS

The authors thank Dr. Sang Sung Nam for preparation of [Ga]–ZSM-5 and [Fe]–ZSM-5. The support of the Department of Energy, Office of Basic Energy Science, Division of Chemical Sciences, is gratefully acknowledged.

REFERENCES

1. Mole, T., Anderson, J. R., and Green, G., *Appl. Catal.* **17,** 141 (1985).
2. Sirokman, G., Sendoda, Y., and Ono, Y., *Zeolites* **6,** 299 (1986).
3. Ono, Y., Sendoda, Y., and Kitagawa, H., *J. Pet. Inst. Jpn.*, 77 (1987).
4. Ono, Y., Nakatani, H., Kitagawa, H., and Suzuki, E., *Stud. Surf. Sci. Catal.* **44,** 279 (1989).
5. Kitagawa, H., Sendoda, Y., and Ono, Y., *J. Catal.* **101,** 12 (1986).
6. Inui, T., Makino, Y., Okazumi, F., Nogano, S., and Miyamoto, A., *Ind. Eng. Chem. Res.* **26,** 647 (1987).
7. Inui, T., Makino, Y., Okazumi, F., and Miyamoto, A., *Stud. Surf. Sci. Catal.* **37,** 487 (1988).
8. Kanai, J., and Kawata, N., *J. Catal.* **114,** 284 (1988).
9. Kanai, J., *Stud. Surf. Sci. Catal.* **44,** 211 (1988).
10. Ono, Y., Kitagawa, H., and Sendoda, Y., *J. Chem. Soc., Faraday Trans. 1* **83,** 2913 (1987).
11. Ono, Y., Adachi, H., and Sendoda, Y., *J. Chem. Soc., Faraday Trans. 1* **84,** 109 (1987).
12. Gnep, N. S., Doyamet, J. Y., and Guisnet, M., *J. Mol. Catal.* **45,** 281 (1988).
13. Meriaudeau, P., and Naccaache, C., *J. Mol. Catal.* **59,** L31 (1990).
14. Ono, Y., and Kanae, K., *J. Chem. Soc., Faraday Trans.* **87,** 669 (1991).
15. Shipiro, E. S., Tkachenko, O. P., and Minachev, Kh. M., *in* "Symposium on Alkylation, Aromatization, Oligomerization and Isomerization of Short Chain Hydrocarbons over Heterogeneous Catalysts," p. 746. Division of Petroleum Chemistry, ACS Meeting, New York, Aug. 25–30, 1991.
16. Guisnet, M. R., Aittaleb, D., Doyemet, J. Y., and Gnep, N. S., *in* "Symposium on Alkylation, Aromatization, Oligomerization and Isomerization of Short Chain Hydrocarbons over Heterogeneous Catalysts," p. 668. Division of Petroleum Chemistry, ACS Meeting, New York, Aug. 25–30, 1991.
17. Kanazirov, V., Price, G. L., and Dooley, K. M., *J. Chem. Soc. Chem. Commun.* **9,** 712 (1990).
18. Le Van Mao, R., and Dufresne, L., *Appl. Catal.* **52,** 1 (1989).
19. Yao, J., Le Van Mao, R., and Dufresne, L., *Appl. Catal.* **65,** 175 (1990).
20. Le Van Mao, R., Dufresne, L., and Yao, J., *Appl. Catal.* **65,** 143 (1990).
21. Le Van Mao, R., Yao, J., and Bijariel, B., *Catal. Lett.* **6,** 23 (1990).
22. Le Van Mao, R., Dufresne, L., Yao, J., and Ly, D., *in* "Symposium on Alkylation, Aromatization, Oligomerization and Isomerization of Short Chain Hydrocarbons over Heterogeneous Catalysts," p. 716. Division of Petroleum Chemistry, ACS Meeting, New York, Aug. 25–30, 1991.
23. Fujimoto, K., Nakamura, I., and Yokota, K., *Chem. Lett.*, 681 (1989).
24. Dmitriev, R. V., Schevchenko, D. P., Shipiro, E. S., Dergachev, A. A., Tkachenko, O. P., and Minachev, Kh. M., *in* "Zeolite Chemistry and Catalysis" (P. A. Jacobs, N. I. Jaeger, L. Kubelkova, and B. Wichterlova, Eds.), p. 381. Elsevier, Amsterdam, 1991.
25. Uemiya, S., Koike, I., and Kikuchi, E., *Appl. Catal.* **76,** 171 (1991).
26. Happel, J., Blanck, H., and Hamill, T. D., *Ind. Eng. Chem. Fundam.* **5,** 289 (1966).
27. McDonald, W. R., and McIntyre, A. D., U.S. Patent 3.119.111, 1964, from *Chem. Abstr.* **60,** 9088 (1964).
28. Stepanov, G. A., Tsailingold, A. L., Levin, V. A., and Pilipenko, F. S., *Stud. Surf. Sci. Catal.* **7,** 1293 (1981).
29. Doroshenko, V. A., Shapovalova, L. P., and Tmenov, D. N., *Z. Prikl. Khim* **55,** 80 (1982).
30. Chaar, M. A., Patel, D., Kung, M. C., and Kung, H. H., *J. Catal.* **105,** 483 (1987).
31. Patel, D., Andersen, P. J., and Kung, H. H., *J. Catal.* **125,** 132 (1990).
32. Singh, D., Gehlawat, J. K., and Rao, M. S., *J. Chem. Tech. Biotechnol.* **47,** 127 (1990).
33. Shenoy, S. C., and Rao, M. S., *J. Chem. Tech. Biotechnol.* **36,** 95 (1986).
34. Shenoy, S. C., and Rao, M. S., *J. Chem. Tech. Biotechnol.* **36,** 110 (1986).
35. Luk'yanenko, V. P., Shapovalova, L. P., Kutnyaya, M. Yu., and Solodkaya, V. S., *J. Appl. Chem. USSR* **60,** 1101 (1987).
36. Doroshenko, V. A., Shapovalova, L. P., and Dolya, L. P., *J. Appl. Chem. USSR* **59,** 1100 (1986).
37. Iton, L. E., Beal, R. B., and Hodul, D. T., *J. Mol. Catal.* **21,** 151 (1983).
38. Alis, G. C., Frenken, P., de Boer, E., Swolfs, A., and Hefni, M. A., *Zeolites* **7,** 319 (1987).
39. Nam, S. S., "Isomorphous Substitution in Zeolites." Ph.D. Dissertation, University of Connecticut, Storrs, CT, 1992.
40. Xu, W.-Q., Suib, S. L., and O'Young, C.-L., *J. Catal.*, in press.